CHARACTERIZATION OF NATURAL STONES EMPLOYED IN HISTORICAL BUILDINGS: A CASE STUDY OF THE FORT IKOMA HISTORICAL BUILDING IN SERENGETI NATIONAL PARK, TANZANIA

Rajab Ayubu Chuo[1*, 2], Patrice Nyangi[1,] and Gislar Kifanyi[1]

[1] Civil Engineering Department, Mbeya University of Science and Technology, P.O. Box 131, Mbeya, Tanzania.

[2] Department of Infrastructure, Tanzania National Parks, P.O. Box 3134, Arusha, Tanzania.

* E-mail address: rajabchuo58@gmail.com (Corresponding author)

Abstract

This study characterizes the natural stones used in the construction of the Fort Ikoma historical building located in Serengeti National Park, Tanzania. The research aimed to support conservation and restoration by analysing the physical, chemical, mineralogical, and petrographic properties of the building stones. Twenty-five samples were examined through field inspections and laboratory techniques, including Energy Dispersive X-ray Fluorescence (EDXRF), X–ray Diffraction (XRD), and petrographic microscopy. Results indicated two dominant stone types: shale and limestone. Shale displayed high silica content, low porosity, and mineralogical components such as quartz, illite, and dickite, making it suitable for superstructure walling. Limestone exhibited high $CaCO_3$ purity, significant calcite content, and characteristic fossil and micritic textures, confirming its suitability for foundation and floor level applications. The findings provide essential material knowledge for informed restoration strategies and contribute to broader conservation efforts for historical stone masonry structures in protected areas.

Keywords: Heritage conservation, Limestone, Mineralogy, Natural stone characterization, Petrography, Shale.

1. Introduction

Ancient structures typically feature large masonry walls and natural stone. Preserving this stone-built heritage is crucial, so it is essential to develop and study appropriate intervention techniques for both materials and structures (Chastre & Ludovico-Marques, 2018). Masonry is one of the primitive building materials that has been used all over the world for construction since the beginning of the earliest civilizations, due to the simplicity of building techniques and the features that characterize these materials (Amer et al., 2020). Earliest construction embraces immense worth in cultural, historical, and archaeological importance, standing as a testament to the originality of past civilizations and craftsmanship at the global level. These classical milestones, imbued with cultural heritage, historical legacy, and architectural marvels, yield tangible links to the collective identity of historical epochs. The ancient constructional artifacts are considered precious assets that contribute to tourism and foster a deep understanding of construction methodologies practiced throughout antiquity (Ali et al., 2024).

Stone heritage buildings serve as significant evidence of human civilization's history, embodying unique cultural symbols of a nation. They possess important artistic, historical, and scientific research value, contributing to our understanding of heritage and identity (Hatır, 2020; Long et al., 2024). Natural stones, such as building stones, have been broadly used by humans since the dawn of time. It mainly comprises limestone, slate, shale, sandstone, marble, etc. The colours and textures of natural stones depend on the type of rock. The building stones

used for construction must meet the high-quality standards of engineering properties to secure the building against all conditions (Freire-Lista, 2021; Bukhari et al., 2023). Historical or heritage stone-built buildings, cultural heritage artifacts, and monuments are vulnerable due to hazards of all kinds, from anthropogenic to natural (Pereira, 2024). The leading causes of the deterioration of natural stone materials exposed to external conditions and employed as either construction material or decoration are time and atmospheric agents (rain, wind, solar radiation, aggressive atmospheric pollutants, freeze-thaw cycles, crystallization of saline solutions, and growth of organisms) (Pappalardo et al., 2022). Natural stones have been used for years in many historically and culturally significant structures (Pereira & Marker, 2016). Natural stones decay at higher rates over time when placed outside their natural environment. They undergo deterioration processes when exposed to weathering because of their intrinsic properties (porosity, permeability, mineralogy), extrinsic properties (fluid circulation, environment, climatic conditions), and anthropogenic factors. The anthropic hazards can be stopped or prevented before it is too late to face fatal consequences, and natural hazards are inevitable (Pereira, 2024; Hernández et al., 2024). This deterioration can lead to loss of value, loss of physical properties, and, lastly, the ruins of historical buildings. Strategies to prevent or protect the stone-built heritage include that if the replacement of stone is necessary, a major effort should be made to identify the stone that was used originally, ensuring that the replacement does not affect either the aesthetics or the cultural value. This approach is a reality in places where the natural conditions are destroying valuable heritage, and the identification of the stone remains vague (Pereira, 2023). Therefore, studying the characteristics of natural stones to understand their ingenuity can help in conservation and restoration work (Hernández et al., 2024). Stones similar to or closely similar to the original natural stones should be used during conservation and restoration work. The use of incompatible stones can be aesthetically insightful or have structurally and financially damaging consequences (Pereira & Marker, 2016).

Historic buildings are significant structures that hold a vital role in history, encompassing listed churches, ancient palaces, castles, monuments, and more. They are defined by three essential attributes: (i) an appropriate age, which, according to the European legislative framework, is at least 50 to 70 years; (ii) a relatively high degree of physical integrity; and (iii) inherent historical significance. Typically, historical buildings are traditional constructions that may lack specific artistic or aesthetic merit. They are generally constructed using local resources, pre-industrial materials, and traditional techniques, which include rural or vernacular buildings, established building stock, and historical towns. The collective responsibility to preserve these buildings for future generations is universally acknowledged (Tejedor et al., 2022). Historical buildings pose numerous challenges for diagnosis and restoration because of limited construction records, diverse and variable materials, restricted access, and limitations on sample extraction, which hinder the use of modern technical standards and building codes (Cintra et al., 2024). The historical significance of Fort Ikoma, firstly constructed as a stone masonry fort by the Germans and later utilized by the British colonial and Tanzanian post-independence governments, underscores the need for its preservation. Historical stone masonry structures like Fort Ikoma often face risks such as material fatigue, environmental loads, and inadequate original construction techniques (Lourenço, 2002). The historical fabric of such buildings reflects the knowledge and experience of past builders, often devoid of modern scientific and engineering standards (Mustafaraj, 2013).

Fort Ikoma, located in Serengeti National Park (SENAPA), Tanzania, serves not only as an architectural and historical landmark but also as a significant asset with potential economic benefits through tourism. However, the fort has deteriorated significantly due to prolonged neglect and structural weaknesses, necessitating a comprehensive assessment and restoration

plan. The preservation and restoration of historical buildings hold paramount importance for maintaining cultural heritage and ensuring its transmission to future generations (Lucian, 2008). The primary purpose of this study is to assess and develop restoration strategies for the Fort Ikoma Historical Building in SENAPA, Tanzania, focusing on the physical, chemical, mineralogical, and petrographic properties of the natural building stones used in its construction. Understanding the characteristics of the natural building stones and their possible damage and proposing their possible solutions is crucial for developing sustainable conservation and restoration strategies that respect the building's architectural, historical, and cultural significance while ensuring its longevity (Hernández et al., 2024). Mineralogical analysis of shales within the Lower Anambra Basin, Nigeria, was conducted by using an X-ray Diffractometer with the aid of a Radicon MD 10 Diffractometer. The diffractogram interpretation was done by comparing the peaks to standard minerals established by the International Centre for Diffraction Data (ICDD) in 2008 and 2009. Geochemical analysis was conducted by using an Inductive Coupled Plasma Atomic Emission Spectrometer (Perkin-Elmer Elan 6000 or 9000) following Lithium metaborate/tetraborate fusion and dilute nitric digestion, to major oxides and rare earth elements were analysed by Inductively Coupled Plasma (ICP) Mass Spectrometry, and Loss on Ignition (LOI) was determined by measuring the weight loss after heating (Okunlola et al., 2023). The deterioration process of limestone in the Anahita Temple of Kangavar (West Iran), its chemical and mineralogical analysis of stones, characterization of deterioration patterns and processes, and identification of factors influencing the process obtained by on-site and laboratory studies, including optical microscopy, petrography, X-ray fluorescence, X-ray diffraction, and scanning electron microscopy coupled with energy dispersive X-ray spectroscopy methods (Barnoos et al., 2020). Unfortunately, there is limited information concerning the characterization of natural stones used in the Fort Ikoma historical building in SENAPA, Tanzania, through physical, chemical, mineralogical, and petrographic analysis.

This study focused on characterizing the natural building stones used in Fort Ikoma through physical, chemical, mineralogical, and petrographic analyses, providing a basis for sustainable restoration strategies. This research employed modern analytical techniques such as X-ray fluorescence (EDXRF), X-ray diffraction (XRD), and reflected and transmitted light microscopy to characterize the natural stones. The findings from this study will contribute to the understanding of historical construction materials and support the preservation of cultural heritage buildings, maintaining both structural integrity and historical authenticity (Degryse et al., 2002).

2. Architectural background

Fort Ikoma is located in the Ikoma ward of the Serengeti district in the Mara region (36M 0682369 UTM 9769712, Map Datum Arc 1960) as shown in Figure 1 and Figure 2. It is one of many Forts built across Tanzania during the German colonial rule from 1885 to 1918. Unlike other German forts built in urban areas, the Fort Ikoma is situated in an area abundant with wildlife. Administratively, Tanzania National Parks (TANAPA), through SENAPA, is the owner and overseer of the Fort. Throughout its history, the fort has served various purposes, including functioning as a hotel, an army training centre, and an administrative facility. It has also undergone multiple structural and architectural modifications during this time (Chuo et al., 2024).

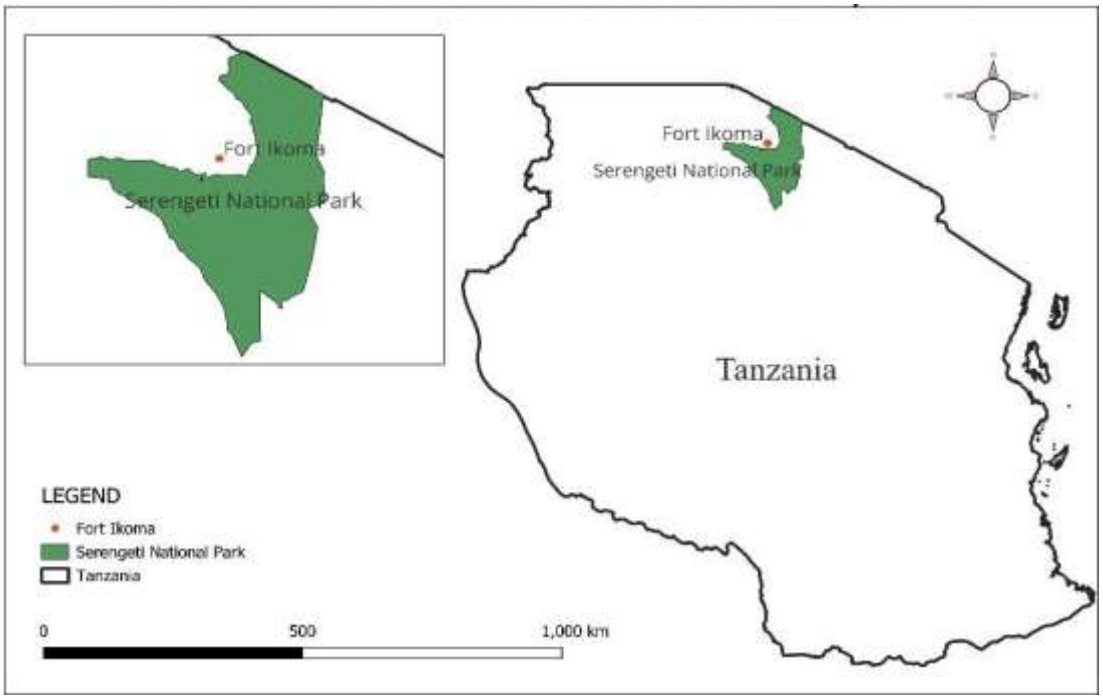

Figure 1: Map showing the location of the Fort Ikoma historical building in SENAPA (Chuo et al., 2024).

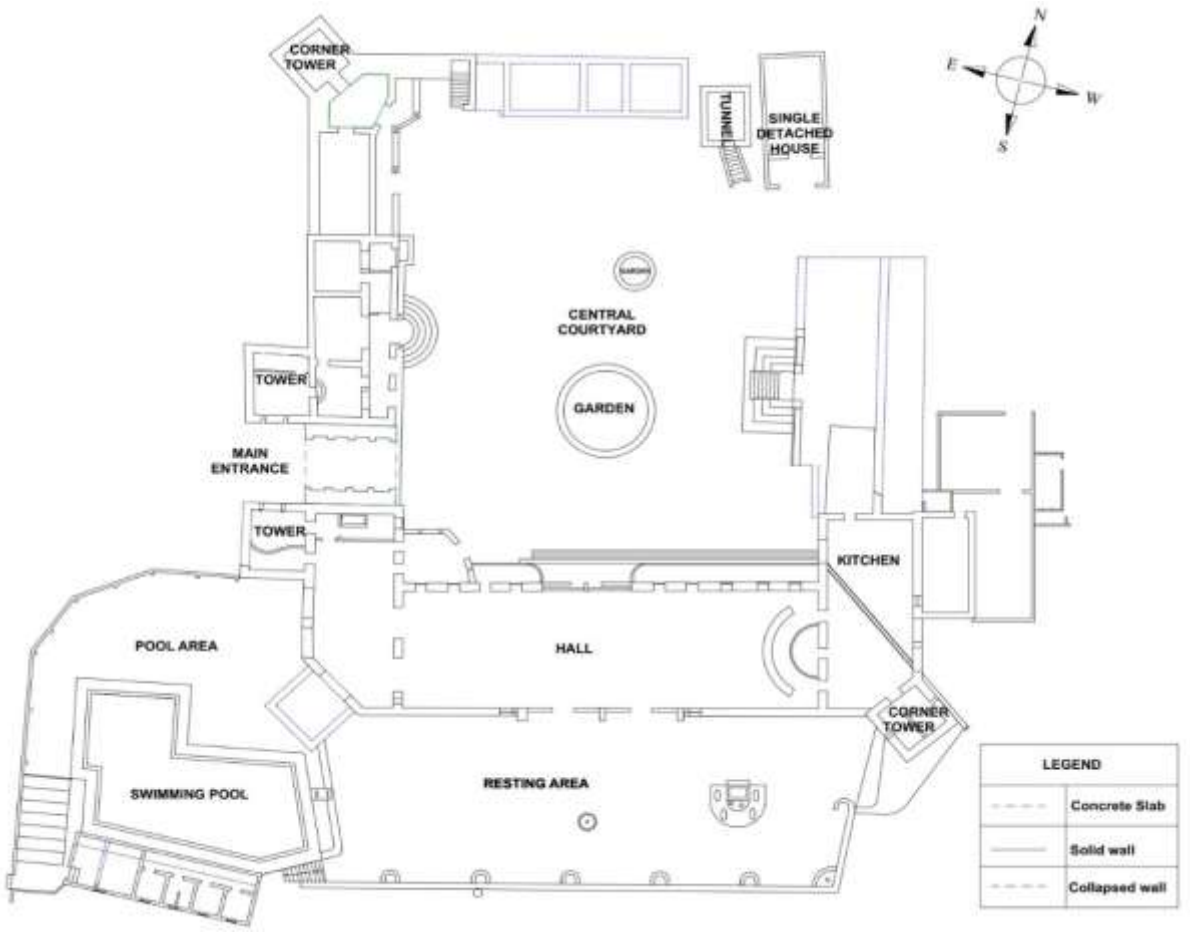

Figure 2: Existing Ground Floor Plan of Fort Ikoma Historical Building in Serengeti National Park (Chuo et al., 2024).

3. Materials and Methods

3.1 Visual Inspections

The study of stone masonry walls has various aims concerning diagnosis and restoration work. The conducted field survey by visual inspection focused on the construction technology of stone masonry walls, building materials, the overall wall thickness, the composition of the inner core layer, and the connectivity between the walls' leaves (Amer et al., 2021).

3.2 Sampling

Through visual investigations, two types of stone materials were identified (sample 1B and sample 2A) (see Figure 3). These samples were collected from areas without aesthetic value or severely damaged parts. The samples (25 numbers) were derived from the outer and inner layers, the ratio between inner and external leaves, the bed and head joints of the outer layer, and the inner core layer (Amer et al., 2021).

Figure 3: Identification of two different natural stone samples used for the construction of the Fort Ikoma historical building in SENAPA, Tanzania.

3.3 Sample Condition and Nature

The samples are grey to reddish brown (1B) and light grey (2A) coloured and composed of clay materials, angular to sub-angular silt to sand-sized grains of quartz and feldspars. The samples have a granular texture; their constituent grains are very fine. These samples were weathered and altered. In this case, prolonged weathering and alteration of the silicate-bearing rocks led to the formation of clay-related minerals. The reddish-brown colour of the shale sample is due to the presence of iron oxide and hydroxide-related minerals**.**

3.4 Physical Characteristics Analysis

The physical characteristics of the stones, including apparent density, moisture content, apparent specific gravity, porosity, and water absorption, were determined according to (CML, 2000; Surdashy & Aqrawi, 2023; the Bureau of Indian Standards, 2003). The stone sample used was crushed into pieces and then passed through the 20 mm IS sieve. The sample, about 1 kg in weight, is washed to make it clean and immersed in a jar of water at room temperature for 24 hours. After 24 hours, the sample is taken out and spread on a cloth to dry its surface, but away from direct sunlight or any heat source, for at least 10 min. The weight of the sample is then measured (B). The sample is again kept in a vessel, and water is poured into it until it shows a 1000 ml mark. The quantity of water added is then recorded (C). The sample is then

taken out of the vessel and dried in an oven at 100°C for a minimum of 24 hours. The weight of the sample is measured after cooling (A) (Patil et al., 2021). Equations (1), (2), (3), (4), and (5) measured the physical characteristics of the natural stone from the Fort Ikoma historical building.

3.4.1 Apparent density (ρ)

Natural stone density is a substantial property and varies in different stones depending on the mineralogy and compaction of the rock. It is usually measured in g/cm^3 (Ali et al., 2023). A natural stone sample's apparent density is defined as the dry sample's mass per unit volume. Compared to wet density values, apparent density tends to vary within narrower limits because the mineral composition and porosity of the natural stone influence it. Natural stones with low porosity and a high proportion of solid components generally exhibit higher dry densities. Moreover, the apparent density of natural stones/rocks increases with depth. Both density and porosity are crucial factors that influence the mechanical properties of the natural stone, as outlined in ASTM C-97-09 (010) (Surdashy & Aqrawi, 2023). The apparent density is calculated using the following equation (1) (CML, 2000).

$$\rho = \left(\frac{A}{((A-Msat)/0.997)}\right) \quad (1)$$

Where: ρ is the apparent density (g/cm³), A is the dry weight of the sample, and Msat is the mass of the saturated sample in water.

3.4.2 Moisture content (M.C)

Water presence in natural stone can alter its properties and behaviour, especially if clay is present, as it softens the material, loosens its structure, and increases deformability, ultimately reducing the stone's overall strength. Water can lower the shear resistance of joint sets, depending on pore water pressure. Rock strength decreases as moisture content rises, making water content a crucial factor influencing natural stone strength (Hagan, 2009). The basic properties of the natural stone influence the durability and elasticity of the natural stone through freezing and thawing processes, moisture content depends on the porosity, density, and permeability of the natural stone and is measured by the weight of the water in the natural stone volume (Ww) to the dry weight of the natural stone volume (Wd) according to ASTM C-127-01 (004), shown in equation (2) (Surdashy & Aqrawi, 2023).

$$M.C = \left(\frac{Ww}{Wd}\right) * 100 \quad (2)$$

Where: M.C.= moisture content

3.4.3 Apparent specific gravity (A.S.G)

The apparent specific gravity of natural stone is the ratio of the mass of a given volume of the natural stone to the mass of a volume of water equal to the volume of the solid matter and impermeable voids of the natural stone (State of California, 2012). Expressed as a numerical value for the saturated surface-dry sample at the recorded temperature, shown in equation (3) (IS 1124-1974, 2003).

$$\text{Apparent specific gravity} = \frac{A}{1000-C} \quad (3)$$

3.4.4 Water absorption (W.A)

Moisture in building materials generally comes from the surrounding environment. This can include humidity in the air, rainfall, capillary action from underground water, and condensation caused by temperature variations. Furthermore, direct and wind-driven rain can directly affect building materials, allowing water to infiltrate through the capillary rise in their pores and

interconnected channels (Li & Gu, 2022). The water absorption of the natural stone is the amount of water absorbed by the natural stone. It is calculated as the ratio of the weight of water absorbed to the weight of the dry material. Expressed as the percentage by weight of the oven-dry sample, shown in equation (4) (IS 1124-1974, 2003).

$$\text{Water absorption} = \left(\frac{\text{B}-\text{A}}{\text{A}}\right) * 100 \quad (4)$$

3.4.5 Apparent Porosity (A.P)

Apparent porosity of natural stone means the ratio of open pores in the natural stone to its total volume of the natural stone. Apparent porosity analysis is the non-destructive analysis of building stones. The porosity is measured with the following equation (5) (Patil et al., 2021);

$$\text{Apparent porosity} = \left(\frac{(\text{B}-\text{A})}{1000-\text{C}}\right) * 100 \quad (5)$$

3.5 Chemical Characteristics Analysis

Chemical characteristics analyses were performed using a Rigaku NEX CG most advanced energy dispersive XRF (EDXRF) spectrometer and it is a non-destructive analysis. The Rigaku NEX CG is an Energy Dispersive X-ray Fluorescence (EDXRF) spectrometer for elemental analysis of Sodium (Na) to Uranium (U) in solid, liquid, and powder samples, as well as thin film coatings on solid substrates. In EDXRF, low-energy "soft" X-rays (1-50 keV) are emitted from an X-ray tube. These source X-rays enter the sample and cause the atoms in the sample to fluoresce their characteristic low-energy "soft" X-rays. These fluorescent X-rays are captured in a detector and counted by a multi-channel analyser. The NEX CG software then calculates the concentration of each element present in the sample from Sodium to Uranium. A powerful and easy-to-use QuantEZ® software interprets XRF with a multilingual user interface.

3.5.1 Calibration of Rigaku NEX CG EDXRF spectrometer

The spectrometer machine was first calibrated using a Multi-Channel Analyzer (MCA) calibration sample to calibrate the relationship between the channels of spectrum data and energy of fluorescent X-rays, and the standard results Fe = 663 keV, Ba = 470 keV, and K = 356 keV were obtained. Then the library calibration was conducted. In the library calibration, the peak profiles of elements are obtained using Sn, Cu, and SiO_2 samples, and the peak profiles are calibrated. The fluorescent X-ray intensities of elements contained in the MCA sample are also obtained to carry out the drift calibration of sensitivity library measurement intensities. If this calibration is not carried out for a long period, library data will not correlate with the data of samples because of variations in peak profiles and X-ray intensities, and erroneous identifications and shifts of analysis value will result. Afterward, sample pellets were loaded and analysed on the EDXRF spectrometer. The obtained sample results were evaluated using NEX CG software, normalized, and finally printed for reporting.

3.6 Limestone Purity Classification

According to Harrison (1993) and Teodorovich (1950), classification, the $CaCO_3$% carried out by the Folks equation (6) (Surdashy & Aqrawi, 2023).

$$\text{CaCO}_3 = \left(\frac{\text{CaCO}_3\text{molecular weight}}{\text{CaO molecular weight}}\right) * \text{CaO}\% \quad (6)$$

3.7 Mineralogical Characteristics Analysis

XRD analysis is a rapid analytical technique mainly used for the phase identification of crystalline minerals and provides information on the sample's unit cell dimensions and chemical composition. In XRD analysis, the X-ray is permitted to pass through each element of the sample, and then deflected. Identification of the elements from the sample is done by this deflection (Patil et al., 2021). Mineralogical characteristics analyses were conducted at ambient temperature using a Rigaku MiniFlex benchtop X-ray diffractometer. The applied equipment conditions were Cu-Kα radiation, λ = 1.5405 Å, from 3 to 70 (2θ) explored range, 0.11 (2θ/s) scanning rate. Its XRD patterns were interpreted using the latest SmartLab Studio–II software, Rigaku's full-function powder diffraction analysis package. The software provides various analysis tools such as automatic phase identification, quantitative analysis, crystallite-size analysis, lattice constants refinement, Rietveld analysis, and ab initio structure determination. The rock samples were first crushed and dried at a temperature of 70 degrees centigrade to reduce moisture content, homogenized, and then split into two parts. One-half was stored for future reference, and the second half was pulverized to get a fine powder of approximately 75 microns.

3.8 Petrographic Characteristics Analysis

Petrographic characteristics analyses were executed using Leica reflected and transmitted light microscopy. A petrographic or thin section was used to analyse the natural stones from the Fort Ikoma historical building. The thin sections were analysed using a Leica DM 750P polarizing light microscope suitable for petrographic analysis due to its high optical resolution.

3.8.1 Thin Section Sample Preparations

The rock chips of 4-5 mm were cut by a diamond-impregnated cutting saw from big to small size rock samples (rock chips), then the rock chips were clearly labelled, dried, and mounted onto glass slides so that two different standard petrographic thin sections were prepared from each sample by using a standard procedure for preparing thin sections. The standard (30 microns) thin sections were made ready for petrographic analysis.

3.8.2 Illustration Images

The images were taken with a Leica camera at X50 magnification; several images were taken at X100 magnification, depending on the features observed. The images were taken at a 1600 x 1200-pixel size at a calibration of 1 pixel = 1 pixel. The field of view for all samples is 7 mm.

4. Results and Discussion

These results were evaluated through EDXRF, X-ray diffraction (XRD), and reflected and transmitted light microscopy tests.

4.1 Visual investigations

Most of the masonry walls were single-leaf and multi-leaf and consisted of three leaves. Two outer leaves (superstructure walling) were well-dressed stones of sample 1B and jointed by mud mortar; the outer leaves of stones were either pointed by cement/sand materials or fully plastered by cement/sand materials of about 0.03 to 0.05 m to protect the wall against weathering effects. The inner core was filled with different samples (1B and 2A). The average wall thicknesses from end to end of the outer leaves were about 0.8 to 1.2 m, with a thickness ratio between external and internal leaves of about 0.10 to 0.25 m. The walls were much thicker at the foundation and floor levels, and wall thickness started to reduce as the height of the superstructure increased. Sample 2A was mostly used on foundation and floor level walling

(see Figure 5). Sample 1B was mostly used on superstructure walling, also in floor slab, stairs, and foundation walling (see Figure 4). Some of the stone walls were observed to be weathered, and some walls collapsed due to long exposure to the weather (see Figure 6).

Figure 4: Superstructure walls that were built by sample 1B.

Figure 5: The foundation wall that was built by sample 2A.

Figure 6: A collapsed superstructure stone masonry wall.

4.2 Physical characteristics

The results of the physical properties of samples 1B and 2A were obtained from the laboratory, as shown in Table 1 and Table 2.

Table 1: Physical properties value of the natural stone sample 1B.

Specimen Reference		**1**	**2**	**3**	**Mean**
Mass of oven-dry aggregate in the air (A)	g	987.10	984.00	985.00	985.37
Mass of saturated surface dry sample + pycnometer	g	1794.00	1792.00	1792.70	1792.90
Mass of saturated surface dry aggregate in the air (B)	g	1026.00	1024.00	1024.00	1024.67
Mass of saturated sample + pycnometer + water	g	2388.00	2368.00	2388.00	2381.33
Quantity of water added (C)	g	594.00	576.00	596.00	588.67
Volume of the pycnometer	g	1000.00	1000.00	1000.00	1000.00
Mass of a clean, dry pycnometer	g	768.00	768.00	768.00	768
Apparent Specific Gravity (A.S.G)	g/cm^3	2.43	2.32	2.44	2.40
Apparent Density (ρ)	g/cm^3	2.70	2.58	2.71	2.66
Water Absorption (W.A)	%	3.94	4.07	3.96	3.99
Apparent Porosity (A.P)	%	9.58	9.43	9.65	9.55
Moisture Content Determination					
Tin Number		**E11**	**E26**	**E58**	**Mean**
Tin + Wet sample (G)	g	391.10	380.30	398.10	389.83
Tin + Dry sample (F)	g	389.10	378.60	396.00	387.90
Water in the sample (G-F) - Ww	g	2.00	1.70	2.10	1.93
Weight of Dry sample (F-T) - Wd	g	302.10	292.40	312.10	302.20
Tin alone (T)	g	87.00	86.20	86.00	86.33
Moisture Content (M.C)	%	0.66	0.58	0.67	0.64

Table 2: Physical properties value of the natural stone sample 2A.

Specimen Reference		**1**	**2**	**3**	**Mean**
Mass of oven-dry aggregate in the air (A)	g	984.70	985.30	988.00	986.00
Mass of saturated surface dry sample + pycnometer	g	1847.00	1845.90	1849.70	1847.53
Mass of saturated surface dry aggregate in the air (B)	g	1071.00	1069.90	1073.70	1071.53
Mass of saturated sample + pycnometer + water	g	2380.00	2380.00	2380.00	2380
Quantity of water added (C)	g	533.00	534.10	530.30	532.47
Volume of pycnometer	g	1000.00	1000.00	1000.00	1000.00
Mass of a clean, dry pycnometer	g	776.00	776.00	776.00	776
Apparent Specific Gravity (A.S.G)	g/cm^3	2.11	2.12	2.10	2.11
Apparent Density (ρ)	g/cm^3	2.60	2.60	2.59	2.59
Water Absorption (W.A)	%	8.76	8.59	8.67	8.67
Apparent Porosity (A.P)	%	18.48	18.16	18.25	18.30
Moisture Content Determination					
Tin Number		**F20**	**F40**	**F36**	**Mean**
Tin + Wet sample (G)	g	490.10	381.30	493.70	455.03
Tin + Dry sample (F)	g	486.40	378.60	490.10	451.70
Water in the sample (G-F) - Ww	g	3.70	2.70	3.60	3.33
Weight of Dry sample (F-T) - Wd	g	399.40	292.40	404.10	365.30
Tin alone (T)	g	87.00	86.20	86.00	86.33

Table 3: Density classification according to ASTM C-97-09, and porosity classification of building stone according to Levorson (1970).

ASTM C-97-09 (010) Classification		**Levorson, 1970 Classification**	
Density g/cm^3	Classification	Porosity %	Classification
< 1.8	Very low	<5	Not present
1.8-2.2	Low	5-10	Low
2.2-2.55	Medium	10-15	Medium
2.55-2.75	High	15-25	High
>2.75	Very high	>25	Very high

4.2.1 Sample 1B

Suitability for building stone in terms of density and porosity according to ASTM C-97-09 (010) and Levorson, 1970 Classification, revealed that sample 1B (ρ = 2.66 g/cm^3 and A.P = 9.55%) was of high density and low porosity, which was recommended as a building stone (Surdashy & Aqrawi, 2023) .

4.2.2 Sample 2A

In terms of density and porosity, according to ASTM C-97-09 (010) and Levorson (1970 Classification of building stone, revealed that sample 2A (ρ = 2.59 g/cm^3 and A.P = 18.30%) was of high density and high porosity, which was accepted as a building stone (Surdashy & Aqrawi, 2023).

All samples revealed that the moisture contents increased as the water absorptions increased, as the increased of porosity of the natural stones increased, the higher value indicated that the materials were highly porous. The durability of the samples depends on water absorption and apparent porosity; the higher the values, the more porous the samples. The minimum moisture content showed that sample 1B was dry compared to sample 2A, with more moisture content. The density increased as apparent specific gravity increased; the higher the amount, the more the natural stone is suitable for construction.

Suitability of limestone rocks in Erbil, Kurdistan Region of Iraq for building stone in terms of dry density and porosity according to ASTM C-97-09 (010) and Levorson, 1970 Classification showed that KF (ρ = 2.02 g/cm^3 and A.P = 15.64%) and QSA (ρ = 2.08 g/cm^3 and A.P = 17.61%) were of low density and high porosity, which were accepted as building stone. Moreover, PtS (ρ = 2.44 g/cm^3 and A.P = 8.63%), SS (ρ = 2.33 g/cm^3 and A.P = 10.50%), HS (ρ = 2.39 g/cm^3 and A.P = 9.00%), and ShS (ρ = 2.22 g/cm^{3}and A.P = 12.14%) were of medium density and porosity, which were highly recommended as building stone, and BQ (ρ = 2.84 g/cm^3 and A.P = 2.90%), SA (ρ = 2.68 g/cm^3 and A.P = 5.20%), PmP (ρ = 2.02 g/cm^{3}and A.P = 15.64%), BK (ρ = 2.02 g/cm^{3}and A.P = 15.64%), and QNE (ρ = 2.64 g/cm^3 and A.P = 6.13%) were of high to very high density and low to no porosity in them, which were recommended as building stone, shown in (see Table 3) (Surdashy & Aqrawi, 2023). Besides, showed that the apparent specific gravity is directly proportional to its dry density, and the amount of water content is directly proportional to its water absorption and porosity (Surdashy & Aqrawi, 2023).

4.3 Chemical Characteristics

The chemical composition analysis results for two stone samples, 1B and 2A, from the Fort Ikoma historical building. The results were provided as percentages for various oxide compounds shown in Table 4.

Table 4: Chemical compositions for samples 1B and 2A (% by weight).

Chemical composition	Sample 1B	Sample 2A
SiO_2	63.27	7.49
Al_2O_3	18.61	2.44
Na_2O	1.00	<0.01
K_2O	3.60	0.30
Fe_2O_3	11.72	1.17
MgO	0.39	0.72
CaO	0.10	87.37
SO_2	<0.01	0.18
TiO_2	1.19	0.15
P_2O_5	<0.01	0.17
BaO	0.12	<0.01
MnO	<0.01	<0.01
SrO	<0.01	<0.01
Cl	<0.01	<0.01

NB: <0.01% means the parameter reading is less than the lowest detection limit, which is 0.01%

4.3.1 Sample 1B

The main chemical leiconstituent of sample 1B was silica (SiO_2) at 63.27%, and other constituents were alumina (Al_2O_3) at 18.61%, iron (III) oxide (Fe_2O_3) at 11.72%, potassium

oxide (K_2O) at 3.6%, titanium oxide (Ti_2O) at 1.19%, and sodium oxide (Na_2O) at 1%. The mean values of chemical analysis results of shales in the Lower Anambra Basin, Nigeria, showed that the predominant chemical composition was silica (SiO_2) at 51.15%, and major constituents were alumina (Al_2O_3) at 15.75%, iron (III) oxide (Fe_2O_3) at 6.83%. Also, the shales were depleted in CaO at 2.35%, MgO at 1.44%, TiO_2 at 1.23%, K_2O at 0.86%, Na_2O at 0.14%, P_2O_5 at 0.11%, and MnO at 0.06% (Okunlola et al., 2023). The sample 1B closely resembled its constituents with Ifon shale from sedimentary basins in Nigeria, whereas showed that the predominantly composition was silica (SiO_2) at 63.30% and other major compositions were alumina (Al_2O_3) at 18.47%, potassium oxide (K_2O) at 2.36%, iron (III) oxide (Fe_2O_3) at 1.26% and titanium oxide (Ti_2O) at 1.02% (Okunlola et al., 2023). Therefore, the possible name of the stone/rock was Shale.

4.3.2 Sample 2A

The sample 2A predominantly chemical constituent was calcium oxide (CaO) at 87.37%, and other constituents were silica (SiO_2) at 7.49%, alumina (Al_2O_3) at 2.44%, and iron (III) oxide (Fe_2O_3) at 1.17%. In the Anahita Temple of Kangavar in West Iran, the XRF analysis of three stone samples from the Temple (samples K3, K4, and K11) revealed that CaO is the primary component, ranging from 32% to 50% by weight, while SiO_2 varies between 2.83% and 11.60% by weight. The high CaO levels indicate the presence of limestone (Barnoos et al., 2020).Therefore, sample 2A's higher CaO composition, at 87.37%, and low composition of MgO at 0.72% indicate that it was limestone (Salvini et al., 2023), and (Dursun, 2024).

4.4 Limestone Purity Classification

Sample 2A's limestone purity classification ($CaCO_3$ approximately 156%) was very high purity ($CaCO_3$% % >98.5) according to the Harrison Classification, and limestone ($CaCO_3$% range between 100-95) according to the Teodorovich Classification, shown in Table 5 below (Surdashy & Aqrawi, 2023). Therefore, sample 2A was a limestone of very high purity.

Table 5: Classification of limestone purity according to the CaCO3 ratio, according to Harrison and Teodorovic

Harrison Classification		**Teodorovich Classification**	
Purity	$CaCO_3$%	Type of rock	$CaCO_3$%
Very High Purity	>98.5	Limestone	100-95
High Purity	97-98.5	Slightly dolomitic Limestone	95-80
Medium Purity	93.5-97	Medium dolomitic limestone	80-65
Low Purity	85-93.5	Highly dolomitic limestone	65-50
Impure	<85	Highly calcitic dolomite	50-35
		Medium calcitic dolomite	35-20
		Slightly calcitic dolomite	20-5
		Dolomite	5-0

4.5 Mineralogical characteristics

The natural stones were analysed by the X-ray diffraction method, and the results are shown below in Table 6.

Table 6: Mineralogical compositions for samples 1B and 2A in volume percentage

Stone Composition		**Sample Name: 1B**		**Sample Name 2A**	
Name	Formula	Major	Minor	Major	Minor
Quartz	SiO_2	30		8.7	
Dickite	$Al_2Si_2O_5(OH)_4$	19			
Illite	$(KH_3O)(AlMgFe)_2(SiAl)_4O_{10}(OH)_2$	12			
Chlorite	$(MgFeAl)_6(SiAl)_4O_{10}(OH)_8$		2.4		
Albite	$NaAlSi_3O_8$		4.5		
Nepheline	$(NaK)AlSiO_4$	5.4			
Hematite	Fe_2O_3		3.6		
Goethite	FeO (OH)		2.0		
Calcite	$CaCO_3$	6.0		64.3	
Sepiolite	$Mg_4(Si_6O_{15})(OH)_2$	7.4			
Rutile	TiO_2		1.0		
Biotite	$K(MgFe)_3(AlSi_3O_{10})\ (FOH)_2$		1.8		
Kaolinite	$Al_2Si_2O_5(OH)_4$		2.1		
Vaterite	$CaCO_3$			6.5	
Siderite	$FeCO_3$				4.8
Dolomite	$Ca(MgCO_3)_2$			5.0	
Diopside	$CaMgSi_2O_6$				3.3
Chloritoid	$(FeMgMn)_2Al_4Si_2O_{10}(OH)_4$		2.8		
Gibbsite	$Al(OH)_3$				2.9
Laumontite	$Ca(AlSi_2O_6)_2$				1.8
Periclase	MgO				1.1
Magnesite	$MgCO_3$				0.6
Muscovite	$KAl_2(AlSi_3O_{10})\ (FOH)_2$				1.0
Total Percentages		**79.8**	**20.2**	**84.5**	**15.5**

4.5.1 Sample 1B

The predominantly stone mineral composition was quartz (SiO_2) at 30% and other major compositions were dickite ($Al_2Si_2O_5(OH)_4$) at 19%, Illite ((KH_3O) $(AlMgFe)_2(SiAl)_4O_{10}(OH)_2$) at 12%, sepiolite ($Mg_4(Si_6O_{15})\ (OH)_2$) at 7.4%, calcite ($CaCO_3$) at 6% and, nepheline (($NaK)AlSiO_4$) at 5.4%. The mineralogical studies of shale conducted in the Lower Anambra Basin, Nigeria, by x-ray diffraction showed that the primary composition was Kaolinite at 41.5%, besides major minerals were montmorillonite, chlorite, and illite; and non-clay minerals were quartz, ilmenite, and sillimanite (Okunlola et al., 2023). Shale is primarily composed of quartz and feldspar, in addition to a variety of major and accessory minerals. The principal minerals identified within shale include kaolinite, illite, and smectite. Furthermore, this sedimentary rock contains minor constituents such as organic carbon, carbonate minerals, iron oxide minerals, sulfide minerals, and heavy minerals, which contribute to its overall composition and characteristics (Dayal, 2017). Therefore, the possible name of the stone/rock was Shale.

4.5.2 Sample 2A

The main stone mineral composition was calcite ($CaCO_3$) at 64.3%, and other major constituents were quartz (SiO_2) at 8.7%, vaterite ($CaCO_3$) at 6.5%, and dolomite (Ca $(MgCO_3)_2$) at 5%. XRD analysis of the three samples (K3, K4, and K11) from the limestone of the Anahita Temple in Kangavar, West Iran, identified calcite ($CaCO_3$) as the predominant

phase in the stone composition. Dolomite ($CaMg(CO_3)_2$) and quartz (SiO_2) were also detected alongside calcite in all the samples. Quartz is a minor phase in many sedimentary and carbonate rocks (Barnoos et al., 2020). The higher mineral constituents of calcite ($CaCO_3$) at 64.3% in sample 2A indicated that it was a limestone. Limestone is a natural mineral primarily composed of calcium carbonate. Some calcium carbonate may have been partially replaced by magnesium carbonate, forming dolomite, which can constitute up to 46% by weight. Many limestones are exceptionally pure, containing less than 5% non-carbonate impurities (Oates, 2008).

4.6 Petrographic characteristics

The results for samples 1B and 2A were analysed as follows;

4.6.1 Sample 1B

General descriptions for sample 1B were;

Mineral assemblage: The rock was grey to reddish brown and composed of 40-50% clay minerals and very fine, round-to-sub round silt-sized quartz grains, opaque isotropic Iron oxide (hematite), and hydroxide (goethite) intergrown with quartz and weathered feldspar and clay matrix, a few flakes of mica minerals, mainly chlorite, biotite, and muscovite. Calcite crystals and very few highly altered plagioclase feldspar grains (colourless, with grey interference colours).

Inclusions: The inclusions were mainly quartz subordinated with highly weathered perthitic K-feldspar and plagioclase feldspar fragments, very few chlorites, and biotite. Few grains of iron oxide and hydroxide, mostly goethite and hematite, and very few altered siderite crystals.

Descriptions: The rock was fine-grained, fissile (splits into thin pieces along the laminations), and laminated (made up of many thin layers), composed of very fine crystals of silt- and clay-sized crystals of clay minerals, angular to sub-angular grains of quartz, and weathered plagioclase feldspars. The rock was characterized by very fine grains of silt and clay particles and a clastic and splintery texture, which makes this rock easily split into thin plates. The rock was formed where mud, silt, and clay-sized mineral crystals were deposited by slow transporting currents and became compacted at the bottom of water bodies. The presence of iron oxide and hydroxide in this rock, such as hematite, goethite, and limonite, which were observed to be isotropic in the microscope, contributed to the reddish-brown colour of this rock. The rock sample was characterized by having a highly weathered plagioclase feldspar grain (colourless, with grey interference colours). Quartz crystals in this sample were fine, round to sub-round, indicating transportation from a certain distance. The muscovite mica was the high-order-coloured strands and strongly pleochroic with basal to perfect cleavage, with the brown grains being biotite mica. Muscovite was colourless at Plane Polarized Light (PPL) and showed high birefringence at Cross Polarized Light (XPL), while Biotite was brown at PPL. The biotite and muscovite flakes were randomly oriented. The grey and colourless grains were quartz and weathered feldspar. The possible name of the stone/rock was Shale. Shale simply splits into thin, mm-scale flakes along the sedimentary bedding, otherwise known as a shaley fissility. Furthermost shales indicate several kinds of grey, showing a high content of clay combined with small amounts of non-oxidized, ferrous iron-rich minerals. Brown or red shale might contain oxidized ferric iron minerals such as hematite (Fe_2O_3). Organic-rich shales were dark grey or black, whereas pale grey and pale green shales (Merriman et al., 2003).

Thin section micrographs: The thin section micrographs description of sample 1B shown in Figure 7 was;

i) 1B(a): Colourless, angular to sub-angular excellent quartz crystals. Iron oxide, mainly hematite, fine crystals in the laminated shale.
ii) 1B(b): Very fine brown biotite crystals with very high pleochroism. Iron oxide (hematite) melt shows a flowing texture surrounding and enclosed in the clay materials (grey with shades).
iii) 1B(c): Yellowish brown weathered plagioclase and perthitic K-feldspar grains (colourless at PPL and with grey birefringence). Colourless quartz crystals and reddish-brown iron oxide.
iv) 1B(d): Very fine calcite crystals (with high reflecting colours at the bottom of the micrography), Clay materials (black), oxide, colourless quartz crystals, weathered plagioclase feldspars, and iron oxide.

4.6.2 Sample 2A

General descriptions for sample 2A were;

Mineral Assemblage: Angular to subangular, poorly sorted, immature fragments of rock composed mainly of calcite, coarse to fine crystals of silt to sand-sized grains of quartz (some stained with iron oxide), altered feldspar (colourless, with grey interference colours), opaque iron oxide grains mainly hematite and magnetite intergrown with quartz and weathered feldspar, fossils, and clay matrix. The rock is medium to coarse-grained and composed of a few microcrystalline calcite matrixes (micrite), some grains of quartz floating in a micritic groundmass, skeletons (fossils), altered siderite, and iron oxide stains.

Inclusions: Inclusions were mainly of calcite, iron oxide, clay materials, and round to sub-round fine to medium quartz, subordinate with highly weathered perthitic K-feldspar and plagioclase feldspar, with very few muscovite and biotite.

Descriptions: The rock was clastic brown and composed mainly of calcite; gravel-sized (greater than 2.5 mm diameter) pebble-sized, of 1.0 cm to 3.5 cm. It had matrix-supported silt to sand-sized, rounded to sub-rounded gravel clasts cemented together, clay materials that fill the spaces between the clasts, and cement them together. The pebbles in the rock were observed to be rounded and soft, indicating they were transported far enough from their source and rubbed against each other. The rock was characterized by fine fracturing and cracking, veinlets of clay materials, carbonaceous grains, and sparry calcite crosscutting fine fractures in a micritic groundmass. Fossils observed in this rock are in parallel and random arrays filled with micrite, which appears to float in micritic groundmass. Most of the cavities were filled with recrystallized calcite, clay materials (black), and a few with iron oxide in a micritic groundmass. There were siderite crystals (grey) observed also in this rock. The clasts in this rock tend to feel smooth and rough when touched. The hardness and colour of this rock are highly variable. Due to the composition of various minerals with different colours and compositions. Calcite in this rock contains euhedral crystals, which form crystal clusters with perfect rhombohedral cleavage and effervescence in cold dilute HCl. Calcite had extremely high birefringence, resulting in pale, washed-out, and white interference colours. Polysynthetic twinning of calcite was also observed. This mineral shows highly variable relief upon stage rotation. Flakes of mica minerals, such as muscovite and biotite, which have a very high pleochroism, were observed. Muscovite was colourless at PPL and showed high birefringence at XPL, while Biotite was brown at PPL. The possible name of the stone/rock was Limestone.

Thin section micrographs: The thin section micrographs description of sample 2A shown in Figure 8 was;

i) 2A(a): Siderite ($FeCO_3$) fragments (colourless at PPL), iron oxide stains in a micritic and sparry calcite groundmass. Cavities are filled with recrystallized calcite and clay materials.
ii) 2A(b): Highly weathered plagioclase feldspar stained with iron oxide, voids filled with clay materials, and fossils floating on clay groundmass. Biotite crystals (brown with strong pleochroism).
iii) 2A(c): Arrays of fossil prints in a micritic and sparry calcite groundmass, highly weathered plagioclase feldspar, quartz, voids filled by recrystallized calcite and clay materials.
iv) 2A(d): Micrite and sparry calcite filled by clay materials; clear quartz crystals were observed. Weathered plagioclase feldspar (yellowish brown) stained with iron oxide, fossils in sparry calcite, and micritic groundmass.

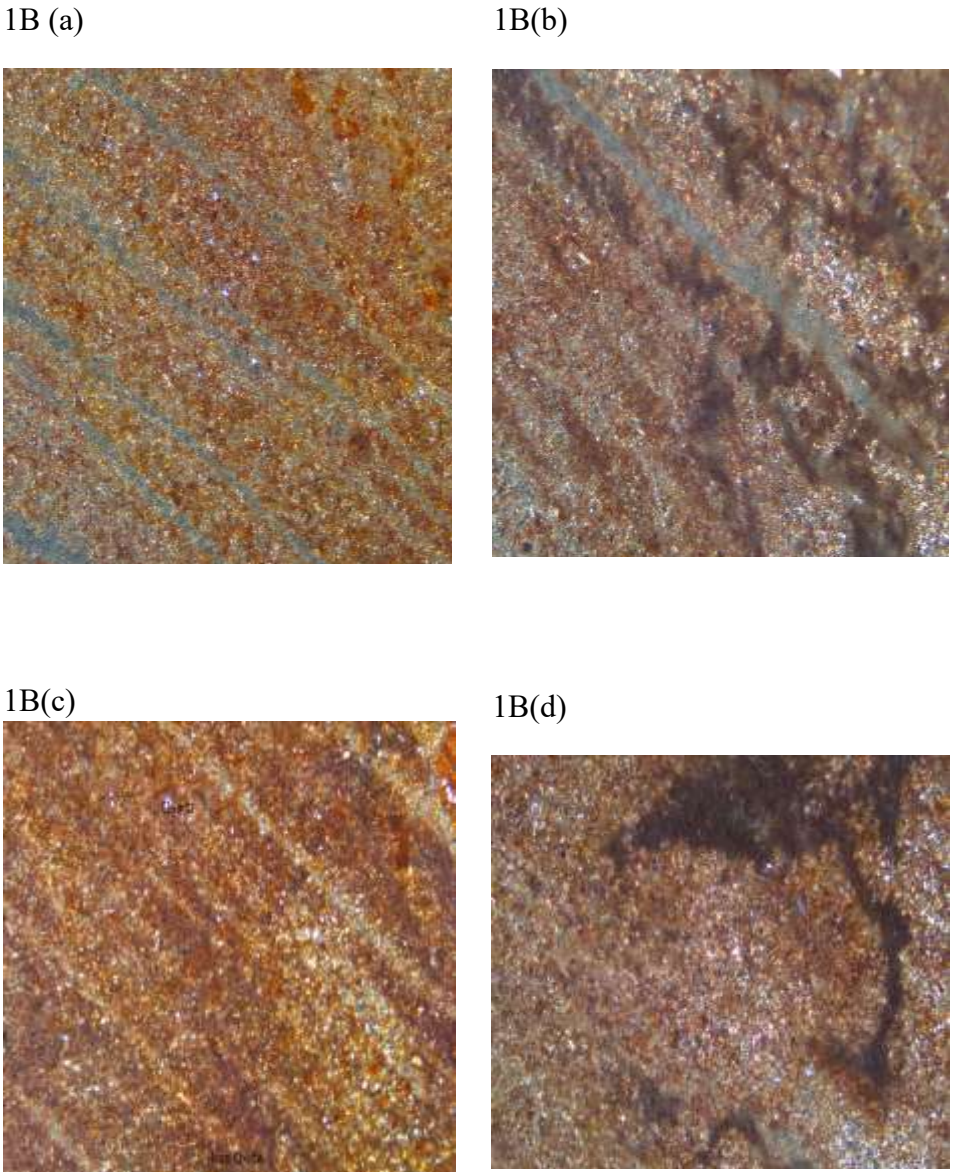

Figure 7: Thin section micrographs of sample 1B.

2A (a)

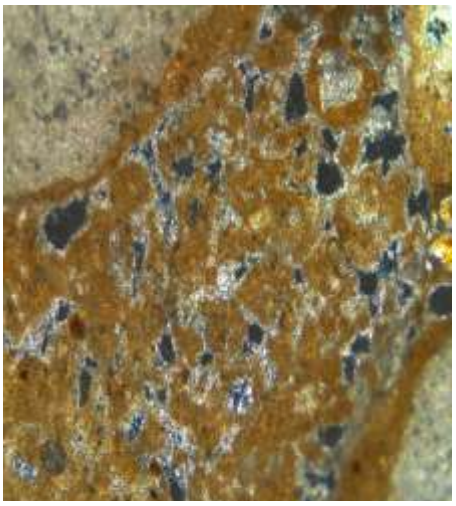

2A(b)

2A(c)

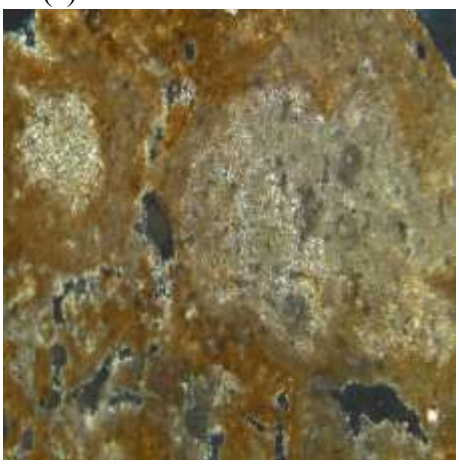

2A(d)

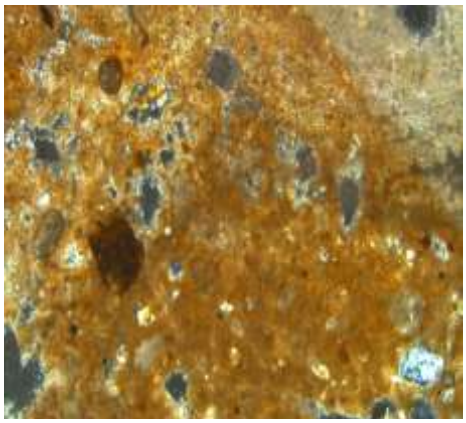

Figure 8: Thin section micrographs of sample 2A.

5. Conclusions and Recommendations

Physical, chemical, mineralogical, and petrographic analysis revealed that the two natural stone samples (1B and 2A) were shale and limestone: shale, recommended as a building stone, was composed of quartz, clay minerals, plagioclase feldspars, iron oxide, and hydroxide, calcite crystals, and mica-related minerals, and limestone, accepted as a building stone was poorly sorted with euhedral siderite grains (with high relief and dark Fe exsolution) and fragments, skeletons, and prints of fossils floating in a fine-grained micritic and sparry calcite groundmass, and characterized by iron oxide stains and occasional voids filled with calcite and clay material. Depositional structures observed include cavities filled with recrystallized calcite, fine fractures filled with iron oxide, iron oxide rims in fossil skeletons and siderite grains, strings of iron oxide cutting across the rocks, and voids filled with clay materials. Clay materials in the two natural stone samples resulted from prolonged extreme weathering of feldspar minerals (known as the mother of clay). Clay materials in these two samples were observed to contain tiny grains of rocks such as quartz and feldspars. When the clay is mixed with water, it becomes

soft, gluey mud that can have various forms. Clay materials are plastic when wet and coherent when dry. It is recommended that the conservation and restoration of the Fort Ikoma historical building in SENAPA, Tanzania, should involve using limestone for the foundation and floor-level walling and shale for the superstructure walling. The findings enhance awareness of historical materials and support the restoration of Fort Ikoma and similar buildings. I recommend that limestone be plastered to increase durability and reduce porosity.

Acknowledgments

The authors would like to thank Burigi-Chato National Park, Serengeti National Park, and the National Museum of Tanzania for permitting them to conduct the research at the Fort Ikoma historical building.

Credit authorship contribution statement

Rajab Ayubu Chuo: Conceptualization, Data curation, Resources, Investigation, Methodology, Formal analysis, Validation, Writing – original draft, Writing – review and editing, Project administration, Funding acquisition. **Patrice Nyangi:** Conceptualization. Writing – review and editing, Supervision. **Gislar Kifanyi:** Conceptualization, Writing – review and editing, Supervision.

Funding: This research received no specific grant from funding agencies in the public, commercial, or not-for-profit sectors.

Data availability: The data used to support the findings of this study are available from the corresponding author upon request.

Ethical approval: All work complies with ethical standards.

Consent to participate: Authors consent to their participation in the entire review process.

Conflict of interest: The authors declare that there is no conflict of interest regarding the publication of this paper.

Consent for publication: The authors give their permission to publish.

References

Ali, B., Khan, M. A., Hanif, M., Anwar, M., Ali, B., Yar, M., & Ahmed, I. (2023). Physico-mechanical and petrographic analysis of the Margalla Hill Limestone, Islamabad, Lesser Himalaya, Pakistan. *Carbonates and Evaporites*, *38:34*(2), 1–12. https://doi.org/10.1007/s13146-023-00858-w

Ali, Castro, J. J., Omi, S., & Nazimi, K. (2024). Exploration and characterization of dynamic properties for cultural heritage conservation: A case study for historical stone masonry buildings in Zanzibar. *Buildings*, *14*(4), 1–23. https://doi.org/10.3390/buildings14040981

Amer, O., Abdel-Aty, Y., El-Hady, M. A., Aita, D., Torky, A., & Hussein, Y. M. (2020). Multiscientific-based approach to diagnosis and characterization of historic stone-masonry walls: The mausoleum of Al-Imam Al-Shafi'i, Cairo (Egypt). *Mediterranean Archaeology and Archaeometry*, *20*(2), 1–16. https://doi.org/10.5281/zenodo.3746944

Amer, O., Aita, D., Mohamed, E. K., Torky, A., & Shawky, A. (2021). Experimental investigations and microstructural characterization of construction materials of historic

multi-leaf stone-masonry walls. *Heritage*, *4*(3), 2390–2415. https://doi.org/10.3390/heritage4030135

Barnoos, V., Oudbashi, O., & Shekofteh, A. (2020). The deterioration process of limestone in the Anahita Temple of Kangavar (West Iran). *Heritage Science*, *8:66*(1), 1–19. https://doi.org/10.1186/s40494-020-00411-1

Bukhari, S. A. A., Basharat, M., Janjuhah, H. T., Mughal, M. S., Goher, A., Kontakiotis, G., & Vasilatos, C. (2023). Petrography and geochemistry of Gahirat marble in relation to geotechnical investigation: Implications for dimension stone, Chitral, Northwest Pakistan. *Applied Sciences (Switzerland)*, *13*(3), 1–14. https://doi.org/10.3390/app13031755

Chastre, C., & Ludovico-Marques, M. (2018). Non-destructive testing methodology to assess the conservation of historic stone buildings and monuments. In *Handbook of Materials Failure Analysis* (1st ed., Vol. 13, pp. 255–294). Elsevier Inc. https://doi.org/10.1016/B978-0-08-101928-3.00013-6

Chuo, R. A., Nyangi, P., & Kifanyi, G. (2024). Chemical, Mineralogical, and Petrographic Analysis of the Mud Mortar from Fort Ikoma Historical Building in Serengeti National Park, Tanzania. *Journal of Applied Sciences and Environmental Management*, *28*(9), 2767–2775. https://doi.org/10.4314/jasem.v28i9.20

Chuo, R., Nyangi, P., & Kifanyi, G. (2024). Condition assessment of heritage structures: The case of Fort Ikoma historical building in Serengeti National Park, Tanzania. *MUST Journal of Research and Development*, *5*(4), 1023–1043. https://doi.org/10.62277/mjrd2024v5i40071

Cintra, D. C. B., Roehl, D. de M., Sánchez Filho, E. de S., Lourenço, P. B., & Mendes, N. (2024). Methodologies for assessing the structural integrity of historic masonry domes and vaults. *IBRACON Structure and Materials Journal*, *17*(4), 1–29. https://doi.org/10.1590/s1983-41952024000400006

Ministry of Works. (2000). *Laboratory testing manual* (1st ed., Vol. 1). The United Republic of Tanzania.

Dayal, A. M. (2017). Shale. In A. M. Dayal (Ed.), *Shale gas: Exploration and environmental and economic impacts* (1st ed., Vol. 1, pp. 1–11). Elsevier.

Degryse, P., Elsen, J., & Waelkens, M. (2002). Study of ancient mortars from Sagalassos (Turkey) in view of their conservation. *Cement and Concrete Research*, *32*(9), 1457–1463. https://doi.org/10.1016/S0008-8846(02)00807-4

Dursun, F. (2024). From quarry to monument: considering Mardin stone (SE, Türkiye) as the symbol of architectural and cultural heritage. *Geoheritage*, *16,64*(3), 1–19. https://doi.org/10.1007/s12371-024-00969-3

Freire-Lista, D. M. (2021). The forerunners on heritage stones investigation: Historical synthesis and evolution. *Heritage*, *4*(3), 1228–1268. https://doi.org/10.3390/heritage4030068

Hagan, P. (2009). A Study on the effect of moisture content on rock cutting performance, in Aziz coal. In P. Hagan (Ed.), *Proceedings of Coal Operators' Conference* (pp. 340–347). University of Wollongong.

Hatır, M. E. (2020). Determining the weathering classification of stone cultural heritage via the analytic hierarchy process and fuzzy inference system. *Journal of Cultural Heritage*, *44*(1), 120–134. https://doi.org/10.1016/j.culher.2020.02.011

Hernández, A. C., Sanjurjo-Sánchez, J., Alves, C., & Figueiredo, C. A. M. (2024). Provenance studies of natural stones used in historical buildings of the Peninsula de Barbanza, Galicia, Spain (North-Western Iberia). *Minerals*, *14,595*(6), 1–17. https://doi.org/10.3390/min14060595

Bureau of Indian Standards. (2003). *Method of test for determination of water absorption, apparent specific gravity, and porosity of natural building stones (IS 1124:1974, reaffirmed 2003)* (1st ed., Vol. 1). Bureau of Indian Standards.

Li, Y.-H., & Gu, J.-D. (2022). A more accurate definition of water characteristics in stone materials for an improved understanding and effective protection of cultural heritage from biodeterioration. *International Biodeterioration & Biodegradation*, *166*, Article 105338. https://doi.org/10.1016/j.ibiod.2021.105338

Long, M., Xu, Z., Chen, Y., Wu, K., & Yang, S. (2024). Conservation of stone heritage buildings: Exploring the algicidal properties of biologically-synthesized nano-silver. *International Biodeterioration & Biodegradation*, *194*, Article 105878. https://doi.org/10.1016/j.ibiod.2024.105878

Lourenço, P. B. (2002). Computations on historic masonry structures. *Progress in Structural Engineering and Materials*, *4*(3), 301–319. https://doi.org/10.1002/pse.120

Lucian, C. (2014). Engineering properties of building materials in historic buildings in Bagamoyo (Tanzania). *Certified International Journal of Engineering and Innovative Technology (IJEIT)*, *3*(9), 2277–3754.

Merriman, R. J., Highley, D. E., & Cameron, D. G. (2003). Definition and characteristics of very-fine-grained sedimentary rocks: clay, mudstone, shale, and slate (commissioned report CR/03/281N). In *British Geological Survey*.

Mustafaraj, E. (2013). Structural assessment of historical buildings: A case study of five Ottoman mosques in Albania. In E. Mustafaraj (Ed.), *Proceedings of 2nd International Balkans Conference on Challenges of Civil Engineering* (pp. 1–13). Epoka University.

Oates, J. A. H. (2008). *Lime and limestone: Chemistry and technology, production and uses* (Vol. 1). John Wiley & Sons.

Okunlola, O., Lydia, A. U., Umaru, A. O., Kazapoe, R. W., & Olisa, O. G. (2023). Mineralogy and geochemistry of shale deposits in the lower Anambra basin, Nigeria: Implication for provenance, tectonic setting and depositional environment. *Economic and Environmental Geology*, *56*(6), 799–816. https://doi.org/10.9719/EEG.2023.56.6.799

Pappalardo, G., Mineo, S., Caliò, D., & Bognandi, A. (2022). Evaluation of natural stone weathering in heritage building by infrared thermography. *Heritage*, *5*(3), 2594–2614. https://doi.org/10.3390/heritage5030135

Patil, S. M., Kasthurba, A. K., & Patil, M. V. (2021). Characterization and assessment of stone deterioration on heritage buildings. *Case Studies in Construction Materials*, *15*(1), 1–25. https://doi.org/10.1016/j.cscm.2021.e00696

Pereira, D. (2023). The value of natural stones to gain in the cultural and geological diversity of our global heritage. *Heritage*, *6*(6), 4542–4556. https://doi.org/10.3390/heritage6060241

Pereira, D. (2024). Stones that tell stories. *Geoheritage*, *16:44*(2), 1–10. https://doi.org/10.1007/s12371-024-00944-y

Pereira, D., & Marker, B. (2016). The value of original natural stone in the context of architectural heritage. *Geosciences (Switzerland)*, *6*(1), 1–19. https://doi.org/10.3390/geosciences6010013

Salvini, S., Coletti, C., Maritan, L., Massironi, M., Pieropan, A., Spiess, R., & Mazzoli, C. (2023). Petrographic characterization and durability of carbonate stones used in UNESCO world heritage sites in northeastern Italy. *Environmental Earth Sciences*, *82*(1), Article 49. https://doi.org/10.1007/s12665-022-10732-y

California Department of Transportation. (2012). California test 106. In *Department of Transportation*. State of California.

Surdashy, A. A., & Aqrawi, A. M. (2023). Evaluation of cretaceous-tertiary limestone for building and dimension stones in Erbil, Kurdistan region of Iraq. *Iraqi Geological Journal*, *56*(2), 48–68. https://doi.org/10.46717/igj.56.2E.4ms-2023-11-9

Tejedor, B., Lucchi, E., Bienvenido-Huertas, D., & Nardi, I. (2022). Non-destructive techniques (NDT) for the diagnosis of heritage buildings: Traditional procedures and futures perspectives. *Energy and Buildings*, *263*, Article 112029. https://doi.org/10.1016/j.enbuild.2022.112029